Design of Nanostructure Complexes by Droplet Epitaxy

ARTICLE *in* CRYSTAL GROWTH & DESIGN · JANUARY 2009

Impact Factor: 4.89 · DOI: 10.1021/cg701142d

4 AUTHORS, INCLUDING:

Ziad Abuwaar
University of Jordan
17 PUBLICATIONS **243** CITATIONS
SEE PROFILE

Gregory Salamo
University of Arkansas
633 PUBLICATIONS **9,149** CITATIONS
SEE PROFILE

CRYSTAL GROWTH & DESIGN
2009
VOL. 9, NO. 2
715–721

Design of Nanostructure Complexes by Droplet Epitaxy

Jihoon H. Lee,[†] Zhiming M. Wang,*[,†] Ziad Y. AbuWaar,[‡] and Gregory J. Salamo[†]

Institute of Nanoscale Science and Engineering, University of Arkansas, Fayetteville, Arkansas 72701, and Department of Physics, University of Jordan, Amman, 11942 Jordan

Received November 20, 2007; Revised Manuscript Received August 27, 2008

ABSTRACT: We demonstrate a number of unseen self-assembled nanostructure complexes fabricated on various GaAs surface indexes by droplet epitaxy. Even under identical growth conditions, the configuration of nanostructure complexes is distinctive on each surface. The morphology evolution of nanostructure complexes is kinetically and energetically analyzed in determining the correlation between shape of nanostructure complexes and atomic surface matrixes with atomic ball−stick models. By systematically varying growth environment, we report many uncanny nanostructure complexes on given surface indexes.

1. Introduction

In the last 15 years considerable effort has been directed toward the growth and control of the size, shape, and distribution of three-dimensional self-assembled nanostructures. Much of this growth effort has taken place using molecular beam epitaxy (MBE), metal organic chemical vapor deposition, and hydride vapor phase epitaxy.[1−5] An outcome of the efforts on these three growth techniques has been the ability to design and engineer size, shape, and distribution of self-assembled nanostructures as well as the energy band gap of nanostructures. This progress has opened the possibility for novel device applications, such as the potential for quantum computing, electron spin memory, quantum dot gates, 'pattern-effect-free' amplification, lasers, photodetectors, and other nanostructure-based applications.[6−10] This understanding and control has also led to interesting nanostructures beyond quantum dots, such as quantum dot molecules, chains, three-dimensional arrays, quantum rings, and other complexes of nanostructures.[11−20] Excitingly, this new ability to design and engineer complex arrays of self-assembled nanostructures is creating new opportunities to explore the underlying physics and potentially lead to novel devices.

One of the most widely used approaches to the self-assembly of nanostructures is the Stransky−Krastanov (S−K) growth mode.[21] In a typical S−K growth mode, self-assembled nanostructures are formed as a result of coherent strain relaxation.[12−14] In this case, the strain is induced by the lattice mismatch between two different material systems such as InAs and GaAs, InP and GaAs, or InN and GaN.[12−14,22] While the S−K growth mode has provided great potential to engineer self-assembled nanostructures, this method is still limited by the nature of the growth mechanism itself, namely the lattice mismatch between the two material systems. To surmount this limitation, another growth approach, the so-called 'droplet epitaxy', has been used as an alternative growth technique to fabricate self-assembled three-dimensional nanostructures.[43,44] For example, droplet epitaxy can be used to fabricate self-assembled nanostructures without a lattice mismatch such as the GaAs/AlAs system.[23−30] In typical III−V droplet molecular beam epitaxy, an atomic flux of a metal is directed onto the surface of a substrate to form liquid droplets, such as Ga, In, and Al droplets. These liquid metal droplets are extremely active to foreign materials, and thus they can be crystallized into high-quality nanocrystals when exposed to an As_4 flux.[15,47] Due to the flexible choice of liquid metal droplets, structures unseen in the past can now be designed and grown. In fact, using this growth approach a very diverse range of nanostructures have been realized such as quantum dot pairs,[29] single and double quantum rings,[17,28] quantum dot molecules,[15] and other configurations of various complex arrays of nanostructures.[18,25,30] Currently, most—if not all—of the designing and engineering efforts of nanostructure complexes adapting droplet epitaxy on the GaAs surface have been performed on the GaAs (100) surface. This very naturally leaves high-index GaAs surfaces as having interesting potential for designing and engineering new complex nanostructures.[31−35]

In this article, we report on the formation of several new complex nanostructures by Ga droplet epitaxy on various GaAs surfaces: (100), (311)A, (711)A, and (731)A. Using MBE, self-assembled liquid droplets are formed on each surface and crystallized into complex GaAs nanostructures with exposure to As_4 flux. Depending on the growth conditions, distinctive shapes of complex GaAs nanostructures are demonstrated on each surface matrix. That is, even under identical growth conditions, each index surface demonstrates a unique complex nanostructure. For example, we observe ring type complex nanostructures on (100), triangular complex nanostructures on (311)A. and 'dot on a disk' nanostructures on (711)A and (731)A surfaces. In fact, we report numerous different complex nanostructures by systematically varying the growth environment on various surface indexes. Moreover, we find that a given surface atomic configuration has a strong correlation with the shape of the complex nanostructure we observe. We carefully explain the underlying growth mechanism that is responsible for the various complex nanostructure in terms of surface diffusion, incorporation of adatoms (surface atoms), and the atomic surface structure that together inherently determines the resulting complex nanostructural configuration. Moreover, the experimental results suggest that various complex nanostructures can find applications in optoelectronics.

2. Experiment

Complex nanostructures were grown by solid source MBE on epitaxy-ready GaAs (100), (311)A, (711)A, and (731)A surfaces. Samples were soldered side by side with indium on a molybdenum holder and degassed for half an hour at 350 °C. Subsequently, the degassed sample holder was introduced into the growth chamber, and surface oxide was thermally desorbed at 600 °C under a beam equivalent pressure (BEP) of 6.4 μTorr of As_4 flux to grow defect-free GaAs buffer.

* Corresponding author. E-mail: arkandream@gmail.com.
[†] University of Arkansas.
[‡] University of Jordan.

10.1021/cg701142d CCC: $40.75
Published on Web 01/09/2009

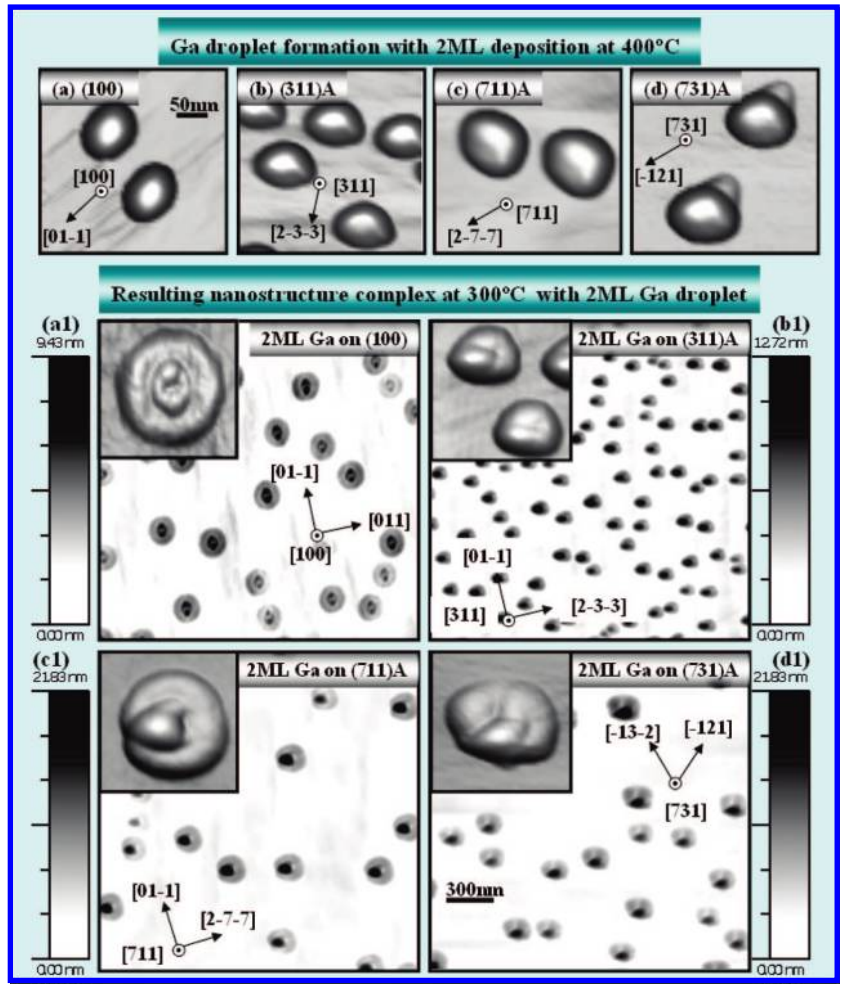

Figure 1. Three-dimensional atomic force microscope (AFM) images of nanostructure complexes and Ga droplets fabricated on each surface index under an identical growth condition (2 ML Ga deposition at 400 °C and crystallized at 300 °C). Panels a−d are 300 × 300 nm, and the scale bar in panel a can be applied for all figures. Panels a1−d1 are 2 × 2 μm^2 areas of plane-view, and the scale bar (300 nm) in panel d1 is equally applied for all figures. The surface index with an equivalent amount of applied Ga is labeled in each picture with applicable Miller indices. Color scale bar with different scales is applied for the height of nanostructures.

A half-micrometer of GaAs buffer was grown at 600 °C under the equally high overpressured As_4 flux. The nominal growth rate of GaAs was one monolayer (ML) per second, which was deduced by an in situ RHEED system. A 10 min annealing period took place to stabilize the GaAs surface directly after buffer growth. Then the As valve was completely closed at around 500 °C to discontinue the As_4 flux, and the substrate temperature was gradually decreased for Ga deposition. At this point, 2 ML of Ga (based on an equivalent amount of GaAs with As_4 flux) was applied to form liquid Ga droplets on the GaAs surfaces at 400 °C without an As_4 flux. While the total amount Ga coverage deposited on different substrate indexes was the same (2 ML), the density, size, and shape of droplets formed on various surfaces were significantly different, which is shown on Figure 1 and discussed in the Results and Discussion section of this manuscript. Then, the Ga droplets were exposed to a BEP of 6.4 μTorr of As_4 flux at 300 °C for 100 s in order to fully crystallize the Ga droplets into GaAs nanocrystals. This growth condition was used for samples in Figures 1 and 2. We systemically varied the amount of the Ga deposition and the As_4 flux as a function of substrate temperature in order to vary surface diffusion and incorporation process for samples shown in Figures 3 and 4. The substrate temperature was quenched right after the termination of each growth under the same BEP of As_4 flux as the crystallization process. Sample surface was exposed without any capping layer, and an atomic force microscope (AFM) in air was used for morphologic analysis.

3. Results and Discussion

In Ga droplet epitaxy, the conversion process from liquid Ga droplets to GaAs nanocrystals, namely exposing active liquid Ga droplets to subsequent As_4 flux, is driven by surface diffusion and incorporation of adatoms (surface atoms).[15,17,45] The direction of diffusion is generally outward from the droplets as the Ga droplets become a Ga source when a flux of As_4 is added onto the surface. The applied flux of As atoms forms a layer of GaAs on the Ga droplet which then diffuses off the droplet. Therefore, the control and/or limitation of surface diffusion and the incorporation of adatoms are the key in designing and engineering the size and shape of nanostructures in droplet epitaxy. Typically, the configuration of nanostructures, specifically the diffusion and incorporation of adatoms, is effectively controlled by controlling the level of As_4 flux within a surface matrix, thus the crystallization process can be enhanced or deterred.[17,28,29] The substrate temperature also plays an important role in designing the size and shape of nanostructures. For example, relatively higher surface diffusion takes place with long-range adatom migration with higher temperatures.[17] GaAs single- and double-ring nanostructures were fabricated on GaAs (100) matrix based on this approach.[17,28]

Figure 1 shows the initial Ga droplets and resulting complex nanostructures on various index surfaces under the identical growth condition of 2 ML of Ga deposition at 400 °C and crystallization at 300 °C. In the formation of complex nanostructures, the size and density of crystallized nanostructures are determined by the size and density of the Ga droplets. The

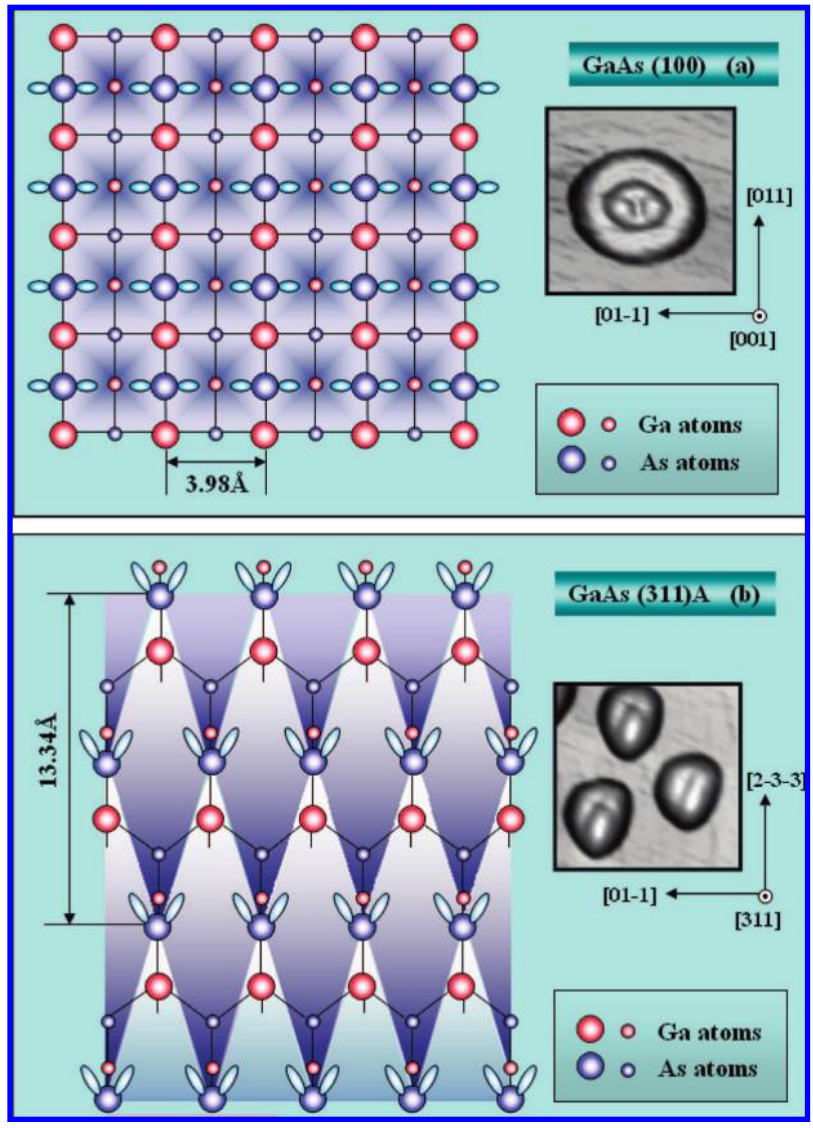

Figure 2. Atomic ball-and-stick models for (a) GaAs (100) and (b) (311)A surfaces with insets (from Figure 1a1,b1) of zoom-in nanostructure complexes grown on each surface. The symmetry between the atomic surface matrixes and grown nanostructure complexes is shown. Three-dimensional AFM insets are 300 × 300 nm. Miller indices are evenly applied for AFM images and atomic models.

configuration of formed nanostructures can be engineered through diffusion process during the crystallization process, but the density is generally strictly determined by the initial droplet density.[17] Despite the identical growth environment, the resulting shape of the Ga droplets differs on each index surface in Figure 1. Figure 1a shows Ga droplets on the GaAs (100) surface with 2 ML deposition. The shape of Ga droplets on GaAs (100) is circular and slightly elongated along [01$\bar{1}$]. The asymmetric shape of Ga droplets on GaAs (100) can be due to an anisotropic surface diffusion of the Ga atoms along [01$\bar{1}$] and [011], which is known to be induced by the asymmetric (2 × 4) surface reconstruction. Due to the surface reconstructed dimmer rows running along [01$\bar{1}$], anisotropic surface diffusion along [011] and [01$\bar{1}$] can be generated.[36,37,46] The average size of the Ga droplets was 80 nm along [011], 95 nm along [01$\bar{1}$], and 13 nm in height. The density of the Ga droplets was ~1.7 × 10^9/cm^2.

The droplets on GaAs (311)A in Figure 1b are triangular, and the density was ~7.6 × 10^9/cm^2 (relatively denser than other surfaces). The average height was 8 nm, and length was 70 nm along [2$\bar{3}\bar{3}$]. In Figure 1c, the shape of Ga droplets on (711)A is somewhat triangular and similar to that on the GaAs (311)A surface. However, the size is much larger and the density is much lower: ~1.1 × 10^9/cm^2. The average height was 10 nm and length was 110 nm along [01$\bar{1}$] and 100 nm along [2$\bar{7}\bar{7}$]. In Figure 1d, Ga droplets on (731)A are also somewhat triangular with a tail running along the direction between [$\bar{1}$21] and [731]. The density was ~1.5 × 10^9/cm^2: about 5 times lower than that on GaAs (311)A. The average height was 14 nm and length was 120 nm along the tail. To sum up, the shape of droplets is circular on GaAs (100) while it is somewhat triangular on the other surfaces but with a tail on (731)A. The density of Ga droplets is a few times higher on (311)A. For more detailed study of droplet formation on various surface indexes, our previous investigations on the formation of Ga droplet with the variation of surface temperature and Ga coverage can provide some useful information.[35]

In designing the shape of resulting GaAs nanostructures in droplet epitaxy, the driving forces, surface diffusion and incorporation, is not only dependent on the growth conditions but also inherently on the surface matrix. Depending on the surface matrix, the surface diffusion and incorporation rate can be highly anisotropic along one direction and/or isotropic for all directions. In Figure 1a1−d1, the resulting GaAs complex

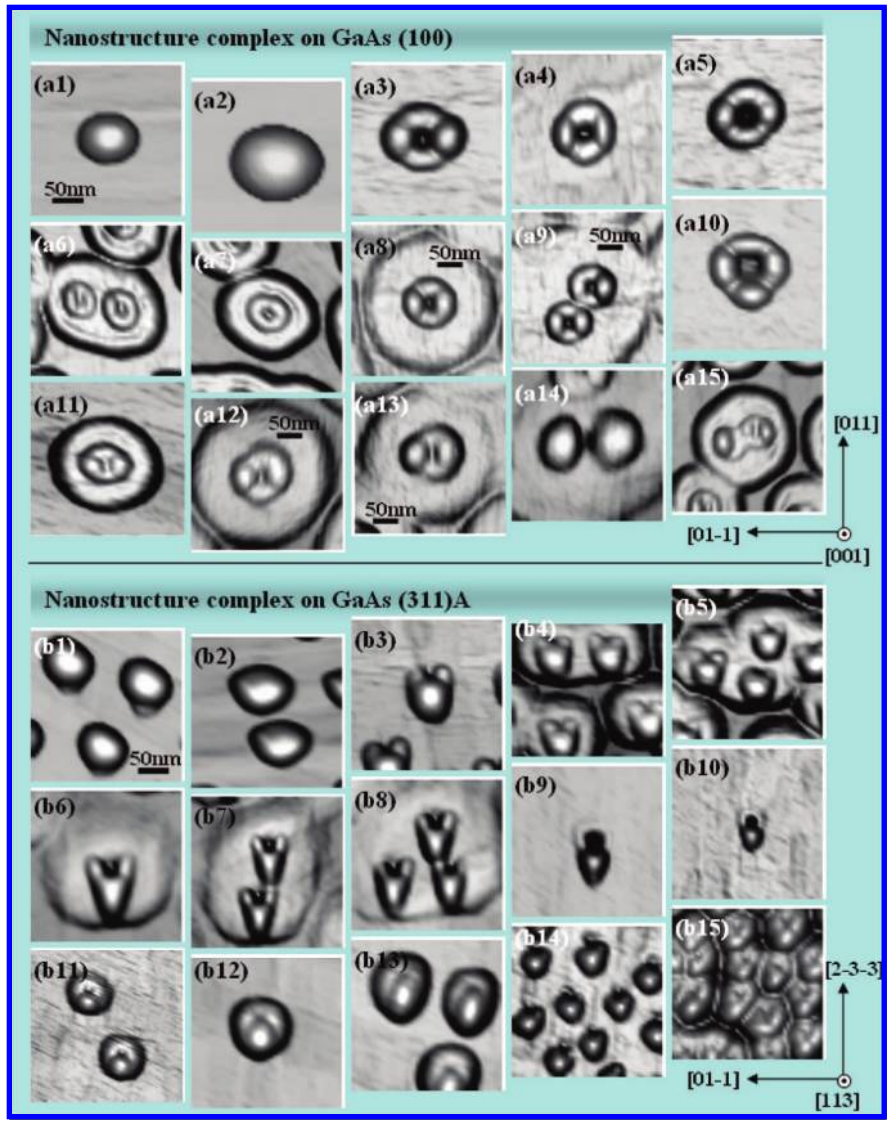

Figure 3. Three-dimensional AFM images of individual nanostructure complexes grown under various growth conditions (various Ga depositions, substrate temperatures, BEP of As_4 fluxes) on the GaAs (100) surface (a3−a15) and on the GaAs (311)A surface (b3−b15). Panels a1, a2, b1, and b2 are droplets. All panels are 250 × 250 nm except a8, a9, a12, and a13 (3000 × 300 nm). The scale bar in panels a1 and b1 can be applied in all figures except larger figures.

nanostructures are, in general, circular on GaAs (100), (711)A, and (731)A surfaces and triangular on the (311)A surface. The resulting nanostructure complex on the GaAs (100) surface in Figure 1a1 is a double-ring-like structure consisting of an inner and outer ring. The average diameter of the outer ring is 200 nm and of the inner ring is 50 nm. The average height of the outer ring is 35 Å and of the inner ring is 50 Å. The inner part of the nanostructure is not a complete ring but in fact has more material along the [01$\bar{1}$] direction, resulting in two dots. Therefore, the height of inner ring differs by 10 Å along the [01$\bar{1}$] and [011] directions. This can be likely due to anisotropic diffusion along the [01$\bar{1}$] and [011] on the GaAs (100) surface during the crystallization, induced by the asymmetric (2 × 4) surface reconstruction.[36,37,46] Figure 2a shows atomic ball−stick models with insets of the complex nanostructures on the GaAs (100) surface. As shown in the atomic ball−stick model in Figure 2a, the GaAs (100) surface is terminated with As atoms with dangling bonds along [01$\bar{1}$], and the unit cell is symmetric along [011] and [01$\bar{1}$].[36,37] Based on the observation of the configuration of the resulting complex nanostructure and by correlating it with the atomic models, we can speculate that the shape of resulting complex nanostructures has a strong relationship with the atomic structure on the surface. For example, the circular shape of resulting complex nanostructures on GaAs (100) appears to be due to the symmetry of atomic configuration of GaAs (100) lattice structure.

Meanwhile, the resulting complex nanostructure on GaAs (311)A in Figure 1b1 is somewhat triangular. The average length of these nanostructures is ∼120 nm along [2$\bar{3}\bar{3}$] and ∼90 nm along [01$\bar{1}$], measuring from the center of the nanostructure. For this complex nanostructure there is a taller dot with two shorter dots along [2$\bar{3}\bar{3}$] on the triangular base. The average height of the tall dot is 90 Å and of the two shorter dots is about 50 Å. Interestingly, the size and shape of the two small dots are very similar. This can be due the symmetric atomic structure on the surface matrix along [01$\bar{1}$].[33,41] Figure 2b shows an atomic ball−stick model for the GaAs (311)A surface. In general, from the singular GaAs (100) surface, GaAs type A surface is cut toward [011] and terminated with As atoms while type B surface is cut toward [01$\bar{1}$] and is terminated with Ga atoms.[38] As seen in Figure 2b, the surface terminated with As atoms has dangling bonds along [2$\bar{3}\bar{3}$]. The upper part of the

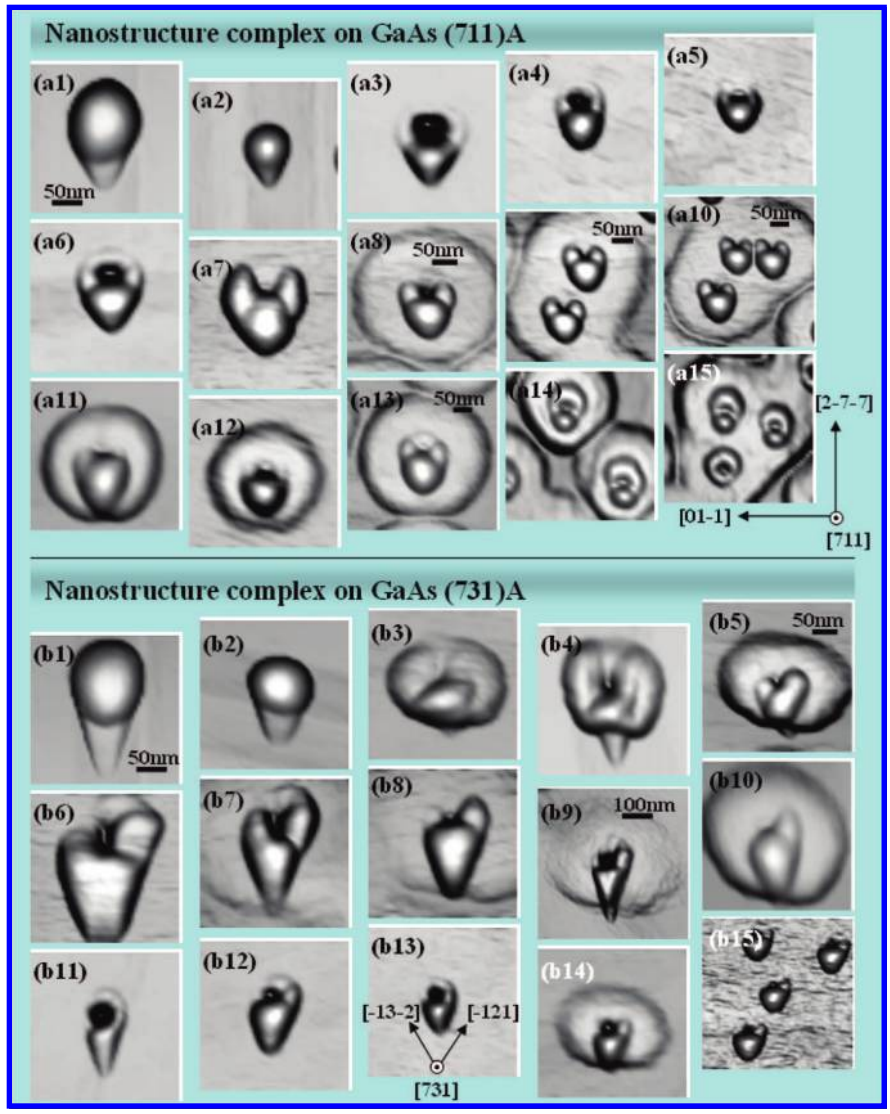

Figure 4. Three-dimensional AFM images of individual nanostructure complexes grown under various growth conditions on the GaAs (711)A surface (a3−a15) and on the GaAs (731)A surface (b3−b15). Panels a1, a2, b1, and b2 are droplets. All panels are 250 × 250 nm except panels a8 (300 × 300 nm), a9 (350 × 350 nm), a10 (400 × 400 nm), a13 (350 × 350 nm), b5 (300 × 300 nm), and b9 (500 × 500 nm). The scale bar in panels a1 and b1 are applied in all figures except larger figures. Miller indices are equally applied for all images.

unit cell is higher and the lower part is deeper, which indicates that the unit cell is symmetric along [01$\bar{1}$] but not along [2$\bar{3}\bar{3}$]. As discussed, the resulting nanostructure complex in Figure 1b1 and in the inset of Figure 2b is symmetric along [01$\bar{1}$], and this again can be due to the symmetry of the atomic surface matrix.[38] Panels c1 and d of Figure 1 show the resulting complex nanostructures on GaAs (711)A and (731)A, respectively. The resulting complex nanostructure is circular. The average size of the ring-like base is 210 nm and that of the height is 6 nm. The inner nanostructure is a heart shape and has an average height of 14 nm. Likewise on the GaAs (311)A surface, the atomic surface matrix of (711)A is symmetric along [01$\bar{1}$].[32] This indicates that the complex nanostructure is symmetric along [01$\bar{1}$]. This symmetry of resulting complex nanostructures along [01$\bar{1}$] on (711)A seems to be due to the symmetry of atomic surface matrix along [01$\bar{1}$].[32,42] In Figure 1d1, the resulting nanostructure complex consists of one big dot and two small dots. The big dot is a near obtuse triangle that is elongated along [$\bar{1}$21]. The average height is 13 nm. Both smaller dots have same average height of 8.5 nm, but the lateral size is obviously larger along [$\bar{1}$21]. This difference in the lateral size, asymmetry of shape, can be due to the anisotropy of the atomic surface matrix on this surface.[34] The GaAs (731)A surface possess high anisotropy of diffusion along [$\bar{1}$21], and thus the resulting structure is larger along [$\bar{1}$21]. From these observations, we find that designing the shape of complex nanostructures is not only dependent on controlling surface diffusion and incorporation of adatom but also strongly related to the atomic surface matrix.

Figures 3 and 4 show various nanostructure complexes on each GaAs surface. The contrast in the AFM images indicates the height variation: brighter means relatively higher in vertical scale, and the darker area indicates relative lower height. The vertical scale of resulting nanostructures after crystallization is up to 15 nm but in general is in between 5 and 10 nm. The growth conditions for these nanostructures were systematically varied, for example, the amount of Ga depositions (1−10 ML), BEP of As_4 fluxes (0.9−6.4 μTorr, 10−100% valve control), and the combination of substrate and crystallization temperatures (200−400 °C). In general, the size of nanostructures showed strong dependence on the initial size of droplets, whose process is mainly governed by the amount of deposition, and BEP of As_4 fluxes during the crystallization as described. However, the

density of nanostructures is mainly dependent on surface temperature.[35] For example, at a fixed surface temperature with the variation of amount of deposition, the density was almost the same but the size of droplets, thus the nanostructures, was further increased, which is described in detail in our previous report on droplet formation on high indexes. For the diffusion process, with high BEP of As_4 fluxes, the surface diffusion is limited, and thus the resulting nanostructures are relatively smaller in lateral scale while the results are reversed with lower BEP of As_4 fluxes, indicating the diffusion is enhanced with lower BEP of As_4 fluxes during the crystallization. This is also well documented in our previous report on ring-shaped nanostructures based on droplet epitaxy.[17]

In Figure 3a, there are in general two types of complex nanostructures on (100). We observe both single-ring-like nanostructures in Figure 3a3−a6 and double-ring-like nanostructures in Figure 3a7−a12. The single-ring-like nanostructures in Figure 3a3−a6 were grown under a relatively high substrate temperature and low As_4 flux, namely high diffusion and incorporation of adatoms and a slow crystallization process. Meanwhile the nanostructures in Figure 3a7−a12 were grown under relatively low diffusion and incorporation and fast crystallization environments. In other words, the diffusion of the outer part of the nanostructure was effectively limited by a low diffusion and incorporation rate as enhanced Ga and As reaction effectively slowed down the diffusion of outer ring. Some of the complex nanostructures such as in Figure 3a13 and a14 are even close to a pair of quantum dots. Figure 3a9 shows closely packed ring-like nanostructures that were observed after a high density of Ga droplets. The diffusion of the outer ring merged together and formed very closely packed nanostructures. Depending on amount of Ga deposition, the size of the Ga droplet can be varied as seen in Figure 3a1 and a2. As discussed with Figure 2a, the atomic surface matrix is symmetric along [011] and [01$\bar{1}$] on GaAs (100); therefore, the resulting complex nanostructures are in general symmetric along both directions on this surface. However, by effectively controlling anisotropic diffusion due to the reconstructed dimmer rows running along [01$\bar{1}$] with the growth parameters, designing of asymmetric complex nanostructures is also possible.

In Figure 3b3−b15, the resulting complex nanostructures on (311)A are generally triangular and symmetric along [01$\bar{1}$] likely due to the symmetry of underlying atomic surface matrix. For example, if we fold the nanostructures along [2$\bar{3}\bar{3}$], we can find the symmetry of these nanostructures along [01$\bar{1}$]. The complex nanostructures in Figure 3b3−b13 are not close to any common geometries and look animal-face-like. For example, they look like a bear Figure 3b3−b5, a dear in Figure 3b6−b8, and a beaver in Figure 3b9 and b13. Depending on the growth parameters, the droplets on this surface can be triangular as well as with a tail in Figure 3b1 and b2. Distinctive nanostructures in Figure 3b14 and b15 have a hole, and these nanostructures can possibly be used for further growth to localize quantum dot and metal particles and study the interaction of metal particles with quantum structures.[39,40]

Figure 4 shows various complex nanostructures grown on GaAs (711)A and (731)A surfaces under systematically varied growth conditions. In general the complex nanostructure complexes on the 711(A) surface are symmetric along [01$\bar{1}$], in a similar way as those on (311)A, and many of them are also animal-face-like. There appear two types of nanostructure complexes. For example, there are singular nanostructures in Figure 4a3−a7 and nanostructures on a circular ring base in Figure 4a8−a15. Singular complex nanostructures were grown under relatively high diffusion and incorporation and slow crystallization, and vice versa for nanostructure complexes on a ring base. While most of the resulting complex nanostructures on GaAs (311)A end up with a singular configuration, many of the complex nanostructures on (711)A have a ring base under identical growth conditions as in Figure 1b1 and c1. This suggests the diffusion and incorporation of adatoms are more favorable on (711)A than on (311)A. In fact, the diameter of resulting nanostructures is smaller on GaAs (311)A as compared to other examined surfaces under identical conditions, which is true for the droplet size, too. In Figure 4b, the resulting nanostructure complexes are also animal-face-like in Figure 4b6−b10 and have a hole in Figure 4b9,b11−b15. Closely looking at these complex nanostructures on GaAs (731), they are distinctive in that many of them have tails and are not symmetric along any direction. For example, the resulting complex nanostructure is larger along [$\bar{1}$21], indicating favorable diffusion along this direction. This can be due to the asymmetry of the atomic surface matrix of this surface.[34] In summary, the symmetry of atomic surface configuration of GaAs (100) seems to be the reason for the symmetry of resulting complex nanostructures. GaAs (311) and (711) have surface matrixes that are symmetric along [01$\bar{1}$] but not along [2$\bar{3}\bar{3}$] and [2$\bar{7}\bar{7}$], and this appears to be the reason for the symmetry of the complex nanostructure along [01$\bar{1}$]. Likewise, the atomic surface matrix of (731) surface is not symmetric along neither [$\bar{1}$3$\bar{2}$] or [$\bar{1}$21] or any direction, so that the formed complex nanostructures are asymmetric along all direction.

4. Conclusions

In conclusion, various shapes of GaAs complex nanostructures are fabricated on GaAs (100), (311)A, (711)A, and (731)A surfaces by droplet epitaxy. Growth conditions were systematically varied to realize various possible sizes and shapes of GaAs complex nanostructures. These complex nanostructures can potentially be used for further growth as a template as well as being able to study cooperative effects among nanostructures. The formation of various nanostructure complexes was discussed in terms of the control on surface diffusion and incorporation of adatoms with the relationship to atomic configurations of surface matrixes. This as well as droplet size in turn primarily determines the size and shape of nanostructure complexes. The key to designing and engineering nanostructure complexes on various GaAs surfaces lies in controlling surface diffusion and incorporation of adatoms and the awareness of the relationship to atomic configuration of surface matrix.

Acknowledgment. The authors acknowledge the financial support of the NSF (Grant DMR-0520550).

References

(1) Hasen, J.; Pfeiffer, L. N.; Pinczuk, A.; He, S.; West, K. W.; Dennis, B. S. *Nature* **1997**, *390*, 54.
(2) Wang, X.; Wang, Zh. M.; Liang, B.; Salamo, G. J.; Shih, C.-K. *Nano Lett.* **2006**, *6*, 1847.
(3) Lee, Y.; Ahn, E.; Kim, J.; Moon, P.; Yang, C,; Yoon, E. *Appl. Phys. Lett.* **2007**, *90*, 033105.
(4) Kiravittaya, S.; Songmuang, R.; Rastelli, A.; Heidemeyer, H.; Schmidt, O. G. *Nanoscale Res. Lett.* **2006**, *1*, 1.
(5) Martin, D.; Napierala, J.; Ilegems, M.; Butté, R.; Grandjean, N. *Appl. Phys. Lett.* **2006**, *88*, 241914.

(6) Onac, E.; Balestro, F.; Willems van Beveren, L. H.; Hartmann, U.; Nazarov, Y. V.; Kouwenhoven, L. P. *Phys. Rev. Lett.* **2006**, *96*, 176601.
(7) Mowbray, D. J.; Skolnick, M. S. *J. Phys. D: Appl. Phys.* **2005**, *38*, 2059.
(8) Li, S.-S.; Long, G.-L.; Baii, F.-S.; Feng, S.-L.; Zheng, H.-Z. *Proc. Natl. Acad. Sci.* **2001**, *98*, 11847–11848.
(9) Stinaff, E. A.; Scheibner, M.; Bracker, A. S.; Ponomarev, I. V.; Korenev, V. L.; Ware, M. E.; Doty, M. F.; Reinecke, T. L.; Gammon, D. *Science* **2006**, *311*, 636.
(10) Liang, C.-T.; Simmons, M. Y.; Smith, C. G.; Kim, Gil.-Ho.; Ritchie, D. A.; Pepper, M. *Appl. Phys. Lett.* **2000**, *76*, 1134.
(11) Saint-Girons, G.; Michon, A.; Sagnes, I.; Beaudoin, G.; Patriarche, G. *Phys. Rev. B* **2006**, *74*, 245305–245310.
(12) Grundmann, M.; Stier, O.; Bimberg, D. *Phys. Rev. B* **1995**, *52*, 11969.
(13) Tersoff, J.; Teichert, C.; Lagally, M. G. *Phys. Rev. Lett.* **1996**, *76*, 1675.
(14) L.G; Wang, P.; Kratzer, N.; Moll, M.; Scheffler, *Phys. Rev. B* **2000**, *62*, 1897.
(15) Lee, J. H.; Wang, Zh. M.; Strom, N. W.; Mazur, Yu. I.; Salamo, G. J. *Appl. Phys. Lett.* **2006**, *89*, 202101.
(16) Bayer, M.; Hawrylak, P.; Hinzer, K.; Fafard, S.; Korkusinski, M.; Wasilewski, Z. R.; Stern, O.; Forchel, A. *Science* **2001**, *291*, 451.
(17) Lee, J. H.; Wang, Zh. M.; Abuwaar, Z. Y.; Strom, N. W.; Salamo, G. J. *Nanotechnology* **2006**, *17*, 3973.
(18) Liang, B. L.; Wang, Zh. M.; Lee, J. H.; Sablon, K.; Mazur, Yu. I.; Salamo, G. J. *Appl. Phys. Lett.* **2006**, *89*, 043113.
(19) Anandan, J. *Science* **2002**, *297*, 1656.
(20) Xu, M. C.; Temko, Y.; Suzuki, T.; Jacobi, K. *J. Appl. Phys.* **2005**, *98*, 083525.
(21) Stranski, I. N.; Krastanov, L. *S-B. Wien Akad. Wiss. (IIb)* **1938**, *146*, 797–810.
(22) Lozano, J. G.; Sánchez, A. M.; García, R.; Gonzalez, D. *Appl. Phys. Lett.* **2006**, *88*, 151913.
(23) Koguchi, N.; Ishige, K. *Jpn. J. Appl. Phys.* **1993**, *32* (5A), 2052.
(24) Gong, Z.; Niu, Z. C.; Huang, S. S.; Fang, Z. D.; Sun, B. Q.; Xia, J. B. *Appl. Phys. Lett.* **2005**, *87*, 093116.
(25) Wang, Zh. M.; Liang, B.; Sablon, K. A.; Lee, J.; Mazur, Y. I.; Strom, N. W.; Salamo, G. J. *Small* **2007**, *3*, 235>238.
(26) Planelles, J.; Climente, J. I. *Eur. Phys. J. B* **2005**, *48*, 65.
(27) Li, S.-S.; Xia, J.-B. *J. Appl. Phys.* **2001**, *89*, 3434–3437. Li, S.-S.; Xia, J.-B. *J. Appl. Phys.* **2002**, *91*, 3227–3231.
(28) Mano, T.; Kuroda, T.; Sanguinetti, S.; Ochiai, T.; Tateno, T.; Kim, J.; Noda, T.; Kawabe, M.; Sakoda, K.; Kido, G.; Koguchi, N. *Nano Lett.* **2005**, *5*, 425.
(29) Yamagiwa, M.; Mano, T.; Kuroda, T.; Tateno, T.; Sakoda, K.; Kido, G.; Koguchi, N.; Minami, F. *Appl. Phys. Lett.* **2006**, *89*, 113115.
(30) Lee, J. H.; Wang, Zh. M.; Liang, B. L.; Sablon, K. A.; Strom, N. W.; Salamo, G. J. *J. Phys. D: Appl. Phys.* **2006**, *40*, 198.
(31) Platen, J.; Kley, A.; Setzer, C.; Jacobi, K.; Ruggerone, P.; Scheffler, M. *J. Appl. Phys.* **1999**, *85*, 3597.
(32) Young, K.; Kahn, A. *J. Vac. Sci. Technol. B* **1986**, *4* (4), 1091.
(33) Wen, H.; Wang, Z. M.; Salamo, G. J. *Appl. Phys. Lett.* **2004**, *84*, 1756.
(34) Temko, Y.; Suzuki, T.; Jacobi, K. *Appl. Phys. Lett.* **2003**, *82*, 2142.
(35) AbuWaar, Z. Y.; Wang, Zh. M.; Lee, J. H.; Salamo, G. J. *Nanotechnology* **2006**, *17*, 4037.
(36) Biegelsen, D. K.; Bringans, R. D.; Northrup, J. E.; −E, L. *Phys. Rev. B* **1990**, *41*, 5701–5711.
(37) Laukkanen, P.; Kuzmin, M.; Perälä, R. E.; Ahola, M.; Mattila, S.; Väyrynen, I. J. *Phys. Rev. B* **2005**, *72*, 045321.
(38) Wang, Zh. M.; Seydmohamadi, Sh.; Lee, J. H.; Salamo, G. J. *Appl. Phys. Lett.* **2004**, *85*, 5031–5033.
(39) Komarala, V. K.; Rakovich, Y. P.; Bradley, A. L.; Byrne, S. J.; Gun'ko, Y. K.; Gaponik, N.; Eychmüller, A. *Appl. Phys. Lett.* **2006**, *89*, 253118.
(40) Gerber, S.; Reil, F.; Hohenester, U.; Schlagenhaufen, T.; Krenn, J. R.; Leitner, A. *Phys. Rev. B* **2007**, *75*, 073404.
(41) Duke, C. B.; Mailhiot, C.; Paton, A.; kahn, A.; Stiles, K. *J. Vac. Sci. Technol. A* **1986**, *4*, 947–952.
(42) Yazdanpanah, V. R.; Wang, Zh. M.; Salamo, G. J. *J. Cryst. Growth* **2005**, *280*, 2–6.
(43) Koguchi, N.; Takahashi, S.; Chikyow, T. *J. Cryst. Growth* **1991**, *111*, 688–92.
(44) Chikyow, T.; Takahashi, S.; Koguchi, N. *Surf. Sci.* **1992**, *267*, 241–244.
(45) Watanabe, K.; Koguchi, N.; Gotoh, Y. *Jpn. J. Appl. Phys.* **2000**, *39*, L79−L81.
(46) Takuji, Y.; Tomonori, M.; Tsutomu, K.; Takashi, K. *Jpn. J. Appl. Phys.* **2005**, *44*, 1397.
(47) Ziad, Y.; AbuWaar, Y. I.; Mazur, J. H.; Lee, Zh. M.; Wang, G. J.; Salamo, *J. Appl. Phys.* **2007**, *101*, 024311.

CG701142D